TISSUE ENGINEERING
Volume 5, Number 5, 1999
Mary Ann Liebert, Inc.

Neural Tissue Formation Within Porous Hydrogels Implanted in Brain and Spinal Cord Lesions: Ultrastructural, Immunohistochemical, and Diffusion Studies

S. WOERLY, M.D., Ph.D.,[1] P. PETROV, M.D., Ph.D.,[1]
E. SYKOVÁ, M.D., Ph.D., D.Sc.,[2,3] T. ROITBAK, M.Sc.,[3] Z. SIMONOVÁ, M.Sc.,[2,3]
and A.R. HARVEY, Ph.D.[4]

ABSTRACT

A biocompatible heterogeneous hydrogel of poly [*N*-(2-hydroxypropyl) methacrylamide] (PHPMA), was evaluated for its ability to promote tissue repair and enhance axonal regrowth across lesion cavities in the brain and spinal cord in adult and juvenile (P17–P21) rats. Incorporation of PHPMA hydrogels into surrounding host tissue was examined at the ultrastructural level and using immunohistochemical techniques. In addition, and in parallel to these studies, diffusion parameters (volume fraction and tortuosity of the gel network) of the PHPMA hydrogels were evaluated pre- to postimplantation using an *in vivo* real-time iontophoretic method. The polymer hydrogels were able to bridge tissue defects created in the brain or spinal cord, and supported cellular ingrowth, angiogenesis, and axonogenesis within the structure of the polymer network. As a result, a reparative tissue grew within the porous structure of the gel, composed of glial cells, blood vessels, axons and dendrites, and extracellular biological matrices, such as laminin and/or collagen. Consistent with matrix deposition and tissue formation within the porous structure of the PHPMA hydrogels, there were measurable changes in the diffusion characteristics of the polymers. Extracellular space volume decreased and tortuosity increased within implanted hydrogels, attaining values similar to that seen in developing neural tissue. PHPMA polymer hydrogel matrices thus show neuroinductive and neuroconductive properties. They have the potential to repair tissue defects in the central nervous system by replacing lost tissue and by promoting the formation of a histotypic tissue matrix that facilitates and supports regenerative axonal growth.

[1]Organogel Canada Ltée, Québec City, QC, Canada.
[2]Department of Neuroscience, 2nd Medical Faculty, Charles University, Prague, Czech Republic.
[3]Institute of Experimental Medicine, Academy of Sciences of the Czech Republic, Prague, Czech Republic.
[4]Department of Anatomy and Human Biology, The University of Western Australia, Nedlands, Perth, WA, Australia.

INTRODUCTION

AXONS OF THE MAMMALIAN CENTRAL NERVOUS SYSTEM (CNS) have the capacity to regenerate following an injury, as shown by long distance regeneration of cut adult central axons along peripheral nerve grafts[1] and by their ability to regrow across CNS microlesions.[2] However, the situation is different when a large lesion is created because the regenerating axons located at the border of the lesion are unable to cross the tissue defect on their own. In this case, the failure of axons to regenerate across the lesion is due to the absence of a cellular and extracellular microenvironment to support axonal growth. For example, axons of the transected spinal cord of the newt grow over significant distances through a neuroepithelial matrix that forms prior to axonal outgrowth.[3] We have previously shown that introducing an artificial hydrogel matrix into large lesions of the double-transected adult rat spinal cord facilitates the reconstitution of an astrocytic, vascular and mesenchymal environment, leading to the formation of a tissue bridge permissive to axonal regeneration.[4] This process of postnatal tissue formation following an injury is named reparative histogenesis, and exists in nature. It occurs by two distinct mechanisms: regeneration by cell division and replacement (e.g., bone marrow), or by tissue reconstitution (e.g., limb regeneration in amphibian).[5] In some non-mammalian vertebrates there is regeneration within the CNS, and regrowth also occurs during embryonic and fetal development in birds and mammals.[6] In those cases, the cascade of postinjury cellular sequences are guided by non-neuronal cellular–extracellular matrices and tissue repair may proceed by an epimorphic-like process for the building of tissue.[3,7–9] The adult mammalian CNS possesses a limited capacity for endogenous repair, as shown by astrocytic differentiation and proliferation, mesenchyme–epithelial interactions, deposition of extracellular matrices, angiogenesis, and axonogenesis.[10–12] In addition, various growth factors that are involved in cell survival, growth cone guidance, axonal outgrowth, and sorting and neuronal connectivity are secreted by the responding cells.[13] Nonetheless, despite an initial attempt to repair a tissue defect, restoration cannot proceed adequately by the single healing process, and the response of the glial and mesenchymal elements leads to a connective tissue scar or pia glial barrier along the lesion.

Various strategies have been used in attempts to repair injured areas of the adult mammalian CNS.[14,15] Cell transplantation has been the most widely investigated strategy, aimed at restoring a tissue defect by exogeneous cell replacement. In contrast, tissue engineering is an emerging field of research and aims at restoring a tissue defect by inducing endogeneous tissue regeneration and manipulating the cascades of cellular events during the healing response. Tissue engineering uses polymer devices with controlled macro- and microstructures and chemical properties to achieve organ regeneration. Ideally, a biohybrid tissue is formed, which becomes a permanent part of the host organ by acting as the functional analogue of the original tissue or organ, and that continues to support tissue functions. Thus, matrices of collagen[16,17] containing neuroactive agents[18] or cell grafts,[19,20] and synthetic polymers including nitrocellulose membranes,[21] tubes of poly (acrylonitrile-vinylchloride),[22] of polycarbonate,[23] of nitrocellulose[24] and polylactide implants[25] have been used for tissue repair of CNS lesions. In particular, the use of porous hydrogel to assist tissue repair and axonal regeneration in the brain[26–31] and the spinal cord[4] has been investigated. Hydrogels that are formed with a three-dimensional network of hydrophilic copolymers are well tolerated by living tissues and may serve as a substrate for tissue formation.[26] The interest in hydrogel as a biomaterial for soft tissue replacement resides in their ability to retain water within the polymer network and also in the possibility to prepare porous matrices that have a controlled porous structure and a specific surface area (e.g., the area delimited by the surface of the polymer network) large enough for cell attachment, growth, and organization and deposition of extracellular matrices. The swollen hydrogel allows for the maintenance of a chemical balance with the surrounding tissue because the water held within the swollen polymer network determines transport properties and allows the exchange between water in the hydrogel and ions and metabolites of tissue fluids. In addition, viscoelastic behavior, low interfacial tension with biological fluids, and structural stability make porous hydrogels suitable for implantation in soft tissue.[32–34] However, key design parameters are needed for application in the CNS for establishing a permissive interface with the host tissue, mobilizing the host's cells within the polymer matrix, and stimulating tissue formation. Thus, a large surface-to-volume ratio, a high fractional porosity of the total polymer network, and mechanical properties that match that of the host tissue are basic requirements. In addition, the pore size distribution should allow infiltration of biological constituents of the host tissue for promoting tissue growth within the

polymer matrix. Hydrogels of poly (*N*-2-hydroxypropyl methacrylamide) (PHPMA) have been synthesized with such properties for stimulating tissue remodelling and organization during natural healing.

In the present study, PHPMA hydrogels were characterized for their porous network geometry (tortuosity) and for their ability to induce tissue formation and axonal regeneration in lesion cavities in the cerebral cortex of young (17 to 21-day-old) rats. As an extension of a previous preliminary study on implantation into the spinal cord,[4] gels were also implanted into a double-transection lesion of the adult rat spinal cord. These models involved the creation of a surgical trauma, the loss of tissue volume, and the implantation of the hydrogel as neural tissue substitute. Using immunocytochemical and ultrastructural methods, tissue infiltration and organization were studied within the PHPMA hydrogels. In a novel approach, we used electrophysiological techniques to measure changes in diffusion parameters (hydrogel-free volume fraction, α; ratio of volume of free spaces for diffusion and total gel volume, and tortuosity of the gel network) within the PHPMA hydrogels from pre- to postimplantation stages, in parallel with the cellular infiltration and formation of a biological matrix in the hydrogel. The dynamic changes were studied *in vivo* using a real-time iontophoretic method, which uses ion-selective microelectrodes to follow the diffusion of an extracellular marker applied by iontophoresis (e.g., tetramethylammonium; TMA).[35] The objectives were to characterize at the structural level tissue formation and axonal regeneration in the PHPMA hydrogel, and to correlate cellular infiltration into the hydrogel network with dynamic physiological changes in diffusion characteristics, and to compare these changes with what is normally seen in adult neural tissue. The results confirm the potential of PHPMA hydrogels to promote tissue repair and axonal regeneration in various types of tissue lesions in the promote tissue repair and axonal regeneration in various types of tissue lesions in the mature and in the developing CNS, and show the stability of the polymer network after implantation.

MATERIALS AND METHODS

Preparation of PHPMA Hydrogels

Macroporous hydrogels (NeuroGel™) were obtained from Organogel Canada Ltd. and were prepared from *N*-(2-hydroxypropyl)-methacrylamide (HPMA) by heterophase separation using radical polymerization in a pore-forming solvent with a divinyl cross-linking agent.

Characterization of the Equilibrium Water Content (EWC)

Gel disks were equilibrated in deionized water at room temperature for 1 week. The gels were blotted with laboratory tissue (to remove surface water), weighed, dried under vacuum at room temperature, and weighed again. The swelling capacity was determined as the mass ratio of water to swollen gel according to the equation: $(W_s\text{-}W_d)/W_s \times 100$, where W_s is the weight of the swollen gel and W_d the weight, of the dried gel. Swelling was calculated as the mean of at least five measurements of different gel samples.

Characterization of PHPMA Hydrogel Structure

Scanning electron microscopy. The structure of the gel was examined by scanning electron microscopy (SEM) after drying the gel using 1,1,1,3,3,3-hexamethyldisilazane (HMDS). The swollen gel was dehydrated through a graded series of ethanol solutions of 70, 85, 95, and 100% for 30 min each. The gel was then immersed in HMDS and air dried in a flow cabinet at room temperature. The dried gel was fractured using a razor blade and was mounted on stubs with colloidal graphite and sputter-coated with gold to an approximate thickness of 200 angstroms. The surface and bulk of gels were examined with a Jeol T 300 SEM using an accelerating voltage of 15 kV.

Transmission electron microscopy. A hydrogel sample was dehydrated and fixed in 2% Osmium Tetroxyde in 0.1 M sodium cacodylate for 1 h at room temperature. The gel was embedded in Epon 812 and ultrathin sections were cut with a Reichert-Jung NOVA ultramicrotom. Gel sections were stained on grids with uranyl acetate and lead citrate. Observations and photomicrographs were made with a JEOL-1200 CX electron microscope operating at 60 kV.

Mercury porosimetry. Pore size distribution, fractional porosity, and specific surface area were determined by mercury porosimetry using a PoreSizer 9320 (Micromeritics) for pressure ranging from 0 to 30 000 psia, as previously described.[26] The porosity was measured on freeze-dried samples and the pore diameter, D, was calculated using the Washburn equation:

$$D = -\frac{4\gamma \cdot \cos\theta}{P},$$

where P is the applied pressure, θ the contact angle (130°) and γ the surface tension (485 dyne/cm) of mercury. The intrusion is the ratio of the injected mercury volume to the volume of the gel.

Pore size distribution within the polymer gel was calculated according to the following equation:

$V(P_a) - V(P_b)/V(\infty) \times 100$
$V(\infty)$ is the volume of intruded mercury at the maximum intrusion at 0.0065 μm
$V(P)$ is the volume of intruded mercury for pore size a and b and $V(Pa) > V(Pb)$.

Porosity was calculated using the equation: $(d_s - d_b) \times 100$, where d_s is the skeletal density of the dried gel (derived from gel volume with the exclusion of the volume of the sample's pore structure) and d_b is the bulk density of the dried gel (derived from the gel volume that includes the volume of the sample's pore structure).

Surface area (i.e., pore wall surface) was computed on the basis of the applied pressure versus intruded volume of mercury using the following equation:

$$A = -\frac{\int_0^{V\max} P \cdot dV}{\gamma \cdot \cos\theta}$$

Animals

Sprague–Dawley or Wistar rats were used in this study. The Sprague–Dawley female rats were obtained from a colony in Quebec; the Wistar rats were obtained from colonies in Prague or in Perth.

Implantation into the Transected Spinal Cord: Ultrastructural Study

The electron microscopy study extended previous light microscopic studies on PHPMA hydrogels implanted into the rat spinal cord.[4] Prior to implantation, the hydrated polymer gels were sterilized in an autoclave at 121°C for 20 min. Three Sprague–Dawley female rats (200–250 g) were used for the ultrastructural study. The animals were anaesthetized by an intraperitoneal injection of ketamine hydrochloride (87 mg/mL) and xylazine (13 mg/mL). Using aseptic surgical techniques, the animals underwent a laminectomy at the thoracic level T9, as previously described.[16] The exposed spinal cord was thoroughly irrigated with a cold saline solution prior to transection. A cordotomy was performed using micro scissors and a 2-mm spinal tissue segment was removed. Following homoestasis, excess clot was washed from the cavity with a chilled saline solution. Cavities of this size was partially filled by a fibrous tissue leaving a central cavity, unless a PHPMA hydrogel is inserted into the cavity to promote the formation of a tissue bridge.[4] The hydrogel implant was sized to adapt to the dimension and shape of the cavity and was inserted into the lesion ensuring complete apposition of the polymer surface with the surfaces of the spinal stumps (this was verified under the surgical microscope at high magnification). Muscles were sutured and the skin closed with wound clips. After surgery, the rats received an intramuscular injection of penicillin G (10,000 U) and a subcutaneous injection of an antalgic (buprenorphine, 0.05 mg/kg). Bladder expression was performed twice a day until recovery of sphincter control. During the first week, the rats were given tetracycline in drinking water to prevent urinary tract infection. The animals were observed daily for spontaneous recovery of locomotor activity and postural function of their hindlimbs during overground locomotion.

After 5 months, the animals were anesthetized and perfused through the heart with a phosphate-buffered saline (PBS) containing heparin followed with paraformaldehyde (4% solution in 0.1 M PBS) and glutaraldehyde (0.4%), and the spinal cords were processed for ultrastructure studies. One spinal cord was cut

longitudinally in the saggital plan. Each hemi-spinal cord was processed either for SEM or for transmission electron microscopy, as described below.

For SEM, the spinal cords containing the hydrogel were dehydrated through ethanol solutions of 70, 85, 95, and 100% for 5 min each. The tissues were then immersed in HMDS for 5 min, air dried at room temperature and mounted on stainless-steel stubs with double sticky tabs. The tissues were then processed and examined as described above.

For transmission electron microscopy (TEM), the spinal tissue block was postfixed in 2.5% glutaraldehyde in 0.1 M sodium cacodylate for 1 h at room temperature and the tissue was embedded in Epon 812. Semi-thin (μm) sections were stained with toluidine blue and ultrathin sections of selected areas were contrasted with uranyl acetate and lead citrate. The sections were observed, as described above.

Implantation in the Cortex of P17 Rats: Immunohistochemical Study

Three P17 rats (Wistar strain) were anesthetized with 2,2,2-tribromoethanol (250 mg/kg, i.p.) and a small lesion cavity (about 2 × 2 × 2 mm) was made in the right frontal cortex region. Cavities of this size are not bridged by new tissue unless matrices are placed in the lesion.[30] A piece of hydrogel sized to the dimensions of the cavity was placed into the lesion site, the bone flap was replaced, superficial wounds were closed and the animals allowed to recover on a heating pad. Seven weeks later, the rats were deeply anesthetized (Nembutal, i.p.) and perfused through the heart with heparinized PBS followed by 4% paraformaldehyde in a phosphate buffer (pH. 7.4). The region of the frontal lobe containing the gel implant was blocked out, sunk in 30% sucrose and 40-μm frozen coronal sections were collected in PBS.

A series of sections was incubated overnight at 4°C with different primary antibodies, all diluted in PBS containing 1% bovine serum albumin (BSA, Sigma, St. Louis, MO) and 0.2% Triton X-100. Primary antibodies used were: Glial Fibrillary Acidic Protein (GFAP; astrocytes; Boehringer, Laval, Quebec, Canada), S100 (astrocytes, Dakopatts, Carpinteria, CA), ED1 (macrophages, Serotec, Raleigh, NC), laminin (Bethesda), RT-97 (neurofilaments; gift of Dr. A. Everett), and growth associated Protein 43 (GAP-43; gift of Dr. G. Wilkin). The dilutions were 1:20 (GFAP), 1:200 (S100, ED1, laminin), 1:100 (RT-97), and 1:1000 (GAP-43). After rinsing (3 × 10 min in PBS), sections were incubated at room temperature with appropriate secondary antibodies (either anti-mouse or anti-rabbit FITC; Sigma) diluted 1:100 in the PBS/BSA/Triton solution. Sections were washed in PBS, mounted onto subbed slides, and then coverslipped with Citifluor.

Implantation in the Cortex of P21 Rats: Extracellular Space Volume Fraction and Tortuosity

To carry out diffusion parameter measurements within the implanted hydrogels, implants were performed in 12 P21 Wistar rats (male and female) weighing 50–60 g. The animals were anesthetized with pentobarbital (60 mg/kg, i.p.) prior to surgery. Small circular holes were made unilaterally at the area of the right frontal cortex (1 mm from midline, bregma 0.2 mm, and interaural 9.2 mm) by aspirating the cortical tissue and a small portion of the white matter. Pieces of hydrogel (1.5–2.0 mm in diameter and length) were placed in the cavity and covered with the cranial bone. The skin overlying the cranium was sutured, and the rats were returned to their cages.

Five to ten weeks after implantation, 10 surviving animals were used in electrophysiological experiments. The rats were anesthetized, as described above, and the brain surface was exposed above the area of implantation by cutting the cranial bones with a dental burr and forceps. A large area of the brain was exposed around the hydrogel implant to allow for control measurements in the host cortex. The meningies were removed, and the head of the animal was restrained in a stereotaxic apparatus. Animals were warmed by a heating pad to maintain body temperature at 37°C. The exposed brain tissue was bathed in warm (37–38°C) artificial cerebrospinal fluid. Electrode penetrations were performed using a step-motor microdrive (Nanostepper, SPI, Oppenheim, Germany). The tracks were made in the area visually identified as hydrogel; control measurements were made 2 to 3-mm distance from the implant. Diffusion curves were recorded from depths of 500 to 3000 μm at 200-μm steps. Only the values from depths of 500–1500 μm (according to the gel size) were included in the statistical analysis. Similar measurements were done in a host cortex before and/or between the gel measurements. Previously, a number of measurements were performed in nonimplanted hydrogels to determine their diffusion characteristics.[4]

TMA^+-selective microelectrodes were used to measure diffusion properties in implanted hydrogels. The ion-selective microelectrodes (ISM) for TMA^+ were made from double-barrel tubing, as described elsewhere.[36] The ion-exchanger was Corning 477317, and the ion-sensing barrel was back-filled with 100 mM TMA chloride while the reference barrel contained 150 mM NaCl. Electrodes were calibrated in a solution of 150 mM NaCl + 3 mM KCl with the addition of TMA^+ at the following concentrations (mM): 0.01, 0.03 0.1, 0.3, 1, 3, and 10. Calibration data were fitted to the Nikolsky equation to determine electrode slope and interference. Iontophoresis pipettes were prepared from theta glass. The shank was bent before back-filling with 100 mM TMA chloride, so that it could be aligned parallel to that of the ISM (Fig. 1). Electrode arrays were made by gluing together an iontophoresis pipette and a TMA^+-selective microelectrode with a tip separation of 140–200 μm. Iontophoresis parameters were a +20-nA bias current (continuously applied to maintain a constant electrode transport number) and a +80-nA current step of 60-sec duration to generate TMA^+ diffusion curves. Potentials recorded at the reference barrel of the ISM were subtracted from the ion-selective barrel measurements by means of buffer and subtraction amplifier. TMA^+ diffusion curves were captured on a digital oscilloscope (Nicolet 310), then transferred to a PC-compatible, 486 computer and analyzed by fitting the data to a solution of the diffusion equation using the VOLTORO program (C. Nicholson, unpublished). TMA^+ concentration-versus-time curves were first recorded in agar gel (0.3% agar solution, Agar Noble, Difco, Detroit, MI) made up in 150 mM NaCl, 3 mM KCl, and 1 mM TMA^+. The iontophoretic curves in agar were used to determine the electrode transport number, n, and free TMA^+ diffusion coefficient, D, (cm^2 sec^{-1}). Diffusion curves were then recorded in nonimplanted hydrogels or in the brain and analyzed to yield a value of α, and TMA^+ apparent diffusion coefficient in tissue, ADC_{TMA}, (cm^2 sec^1), λ, (λ = OD/ADC) and nonspecific TMA^+ uptake, k' (sec^{-1}).[35] These parameters were extracted by a nonlinear curve-fitting

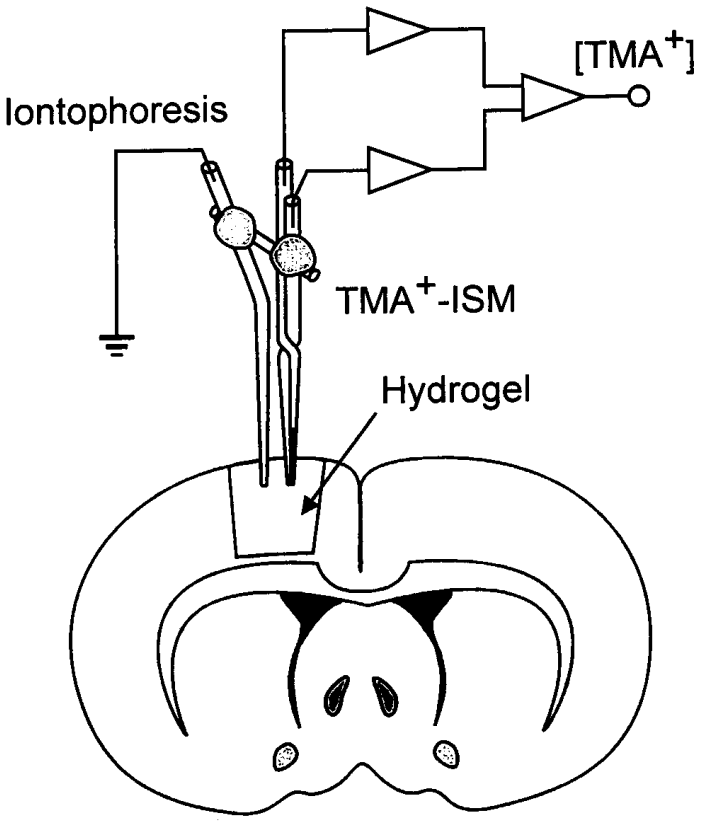

FIG. 1. Experimental arrangement for TMA^+ diffusion measurement in the hydrogel implanted into the rat cortex, showing TMA^+-selective double-barrelled ion-sensitive microelectrode (ISM) and iontophoresis microelectrode. The separation between electrode tips was 140–200 μm. The ISM was connected to a pair of high-impedance buffer amplifiers followed by a subtraction amplifier and connected to a digital oscilloscope and computer.

simplex algorithm operating on the diffusion curve described by Eq. 1, which represents the behavior of TMA^+, assuming that it spreads out with spherical symmetry, when the iontophoresis current is applied for duration S.[35] In this expression, C is the concentration of TMA^+ at time t and distance r. The equation governing diffusion in brain tissue is:

$$C = G(t) \quad t < S, \qquad \text{for the rising phase of the curve;}$$

$$C = G(t) - G(t - S) \quad t > S, \qquad \text{for the falling phase of the curve.}$$

The function $G(u)$ is evaluated by substituting t or $t - S$ for u in the following equation:

$$G(u) = (Q\lambda^2/8\pi D\alpha r) \{\exp[r\lambda(k'/D)^{1/2} \operatorname{erfc}[r\lambda/2 (Du)^{1/2} + (k'u)^{1/2}] + \exp[-r\lambda(k'/D)^{1/2} \operatorname{erfc}[r\lambda/2 (Du)^{1/2} (k'u)^{1/2}]\}. \quad (1)$$

The quantity of TMA^+ delivered to the tissue per second is $Q = In/zF$, where I is the step increase in current applied to the iontophoresis electrode, n is the transport number, z is the number of charges associated with substance iontophoresis (+1 here), and F is Faraday's electrochemical equivalent. The function "efrc" is the complementary error function. When the experimental medium is agar, by definition, $a = 1 = \lambda$ and $k' = 0$, and the parameters n and D are extracted by curve fitting. Knowing n and D, the parameters a, λ and k' can be obtained when the experiment is repeated in the brain or in the gel. The statistical significance of data from nonimplanted hydrogel, implanted hydrogel, and host cortex was evaluated by one-way analysis of variance (ANOVA) test. All data are expressed as mean ± SEM. Figure 1 shows the experimental arrangement for TMA^+ diffusion in the hydrogel implanted into the cortex.

Histological verification of the microelectrode penetration was carried out after each experiment. At the end of the electrophysiological measurements, the anesthetized animals were perfused with 4% paraformaldehyde in 0.1 M PBS (pH 7.5). Brains were fixed for 4 h, then dissected and immersed in PBS with 30% sucrose. Frozen coronal sections (40 μm) were cut, some of them stained with cresyl violet (Nissl), others with monoclonal antibodies to GFAP (Boehringer-Mannheim, Mannheim, Germany), as described above.

RESULTS

Characterization of Hydrogel Structure

The capacity of the PHPMA hydrogel to retain water within its structure was calculated as 95.66% of the swollen weight of the gel. Under TEM, the PHPMA hydrogel shows a "grape-like" structure with clustering of spheroidal particles or microspheres, which have an even distribution in the specimen. At higher magnification, the inner structure of the polymer microspheres presents an open, fine, electron dense network corresponding to micropores (Fig. 2). The peripheral rim of the polymer particles is tightly packed and, depending on the level of sectioning, is more or less thick. Under SEM, the PHPMA gels demonstrate a macrophase separated structure with a three-dimensional network of polymer microspheres of 3- to 5-μm organized in loosely packed contact (Fig. 3A and 3B). The void of the polymer gel was constituted by noncircular macropores delimited by the surface of the microspheres, forming an open interconnected porous system, and the geometry and the topology of the pore space were represented by the spatial arrangement of the sphere network. At higher magnification, SEM showed the presence of mesopores at the surface of the polymer microspheres (Fig. 3C).

Porous properties of the PHPMA hydrogel were determined by mercury porosimetry. The specific surface area shows a value of 40 ± 8 m^2/g and represents the surface area in the range of macropores and mesopores up to 0.0065 μm, which is the limit of detection of the porosimeter used. This value of the pore surface area corresponds to the total surface area generated by the polymer microspheres minus the lower mesopores and therefore we should expect that the total specific surface area of the hydrogel is larger than

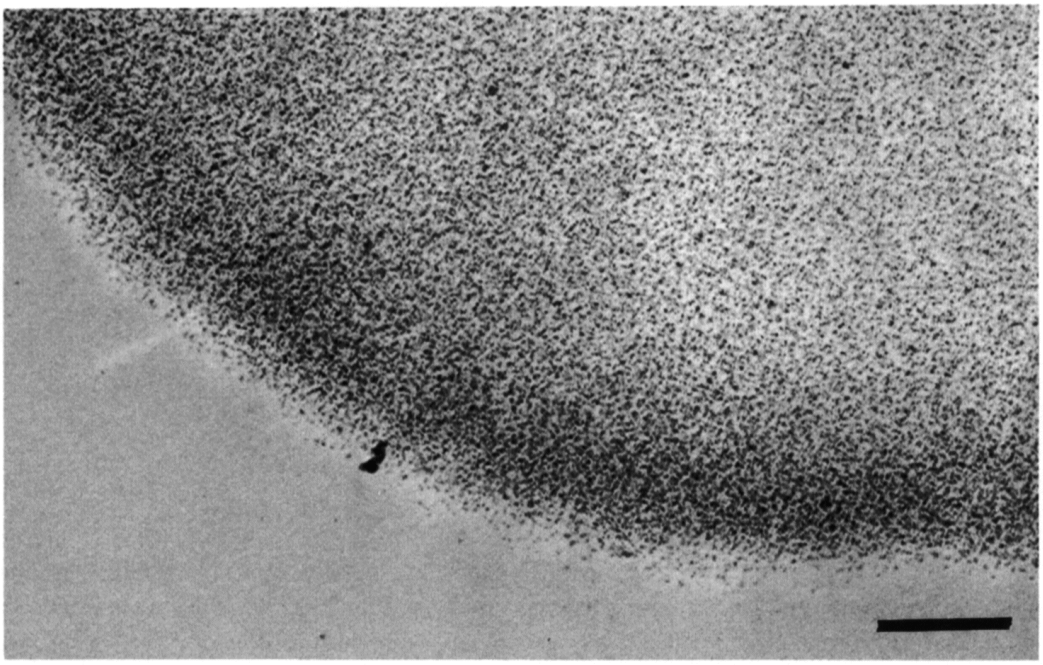

FIG. 2. TEM of a polymer microsphere of the PHPMA hydrogel showing the presence of micropores throughout the polymer gel. Scale bar : 0.2 μm.

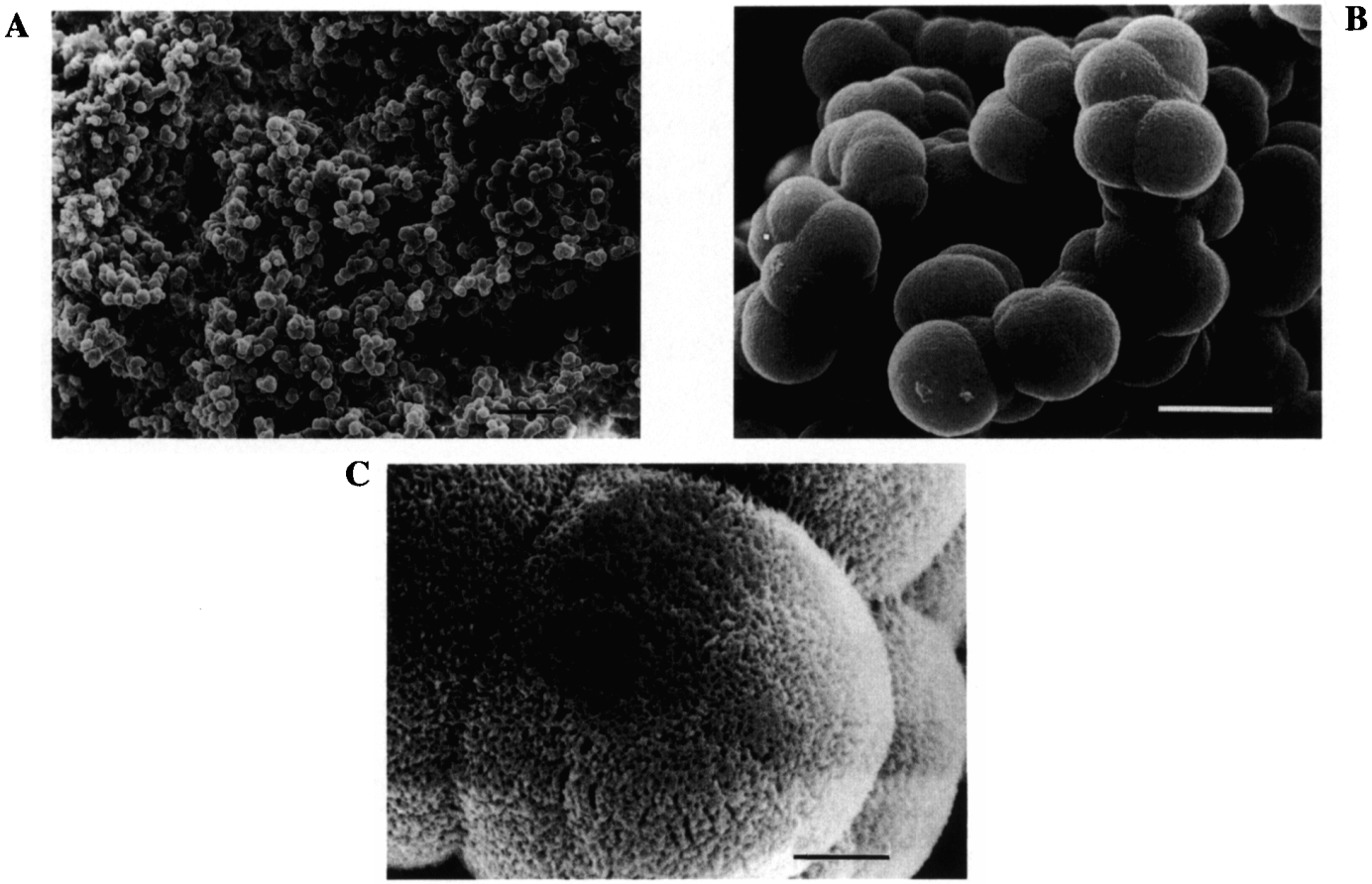

FIG. 3. SEM micrographs of the freeze-dried PHPMA hydrogel at increasing magnification, showing the structure and the spatial arrangement of the macromolecular network constituted by crosslinked polymer microspheres and the associated porous structure (**A** and **B**). (**C**) high power scanning electron microscopy of the hydrogel showing the presence of mesopores at the surface of the polymer microspheres. Scale bars: A = 20 μm; B = 4 μm; C = 1 μm.

the value determined by mercury porosimetry. The mean pore diameter was 22 ± 3 μm and the fractional porosity, which is the porous percentage of volume of the gel, was found equal to 89 ± 2%. Figure 4A shows the cumulative pore size distribution within the pore volume of the gel. It can be seen that the matrix porosity varies as an exponential function of the distribution of pores size. Figure 4B shows that the largest fraction of the porous structure of the hydrogel is constituted of pores between 30- to 10-μm diameter.

Implantation into the Transected Spinal Cord: Ultrastructural Study

A low magnification SEM examination of the implantation site of the spinal cord, 5 months after implantation of the hydrogel, showed the integrity of the PHPMA hydrogel, which had formed a continuous

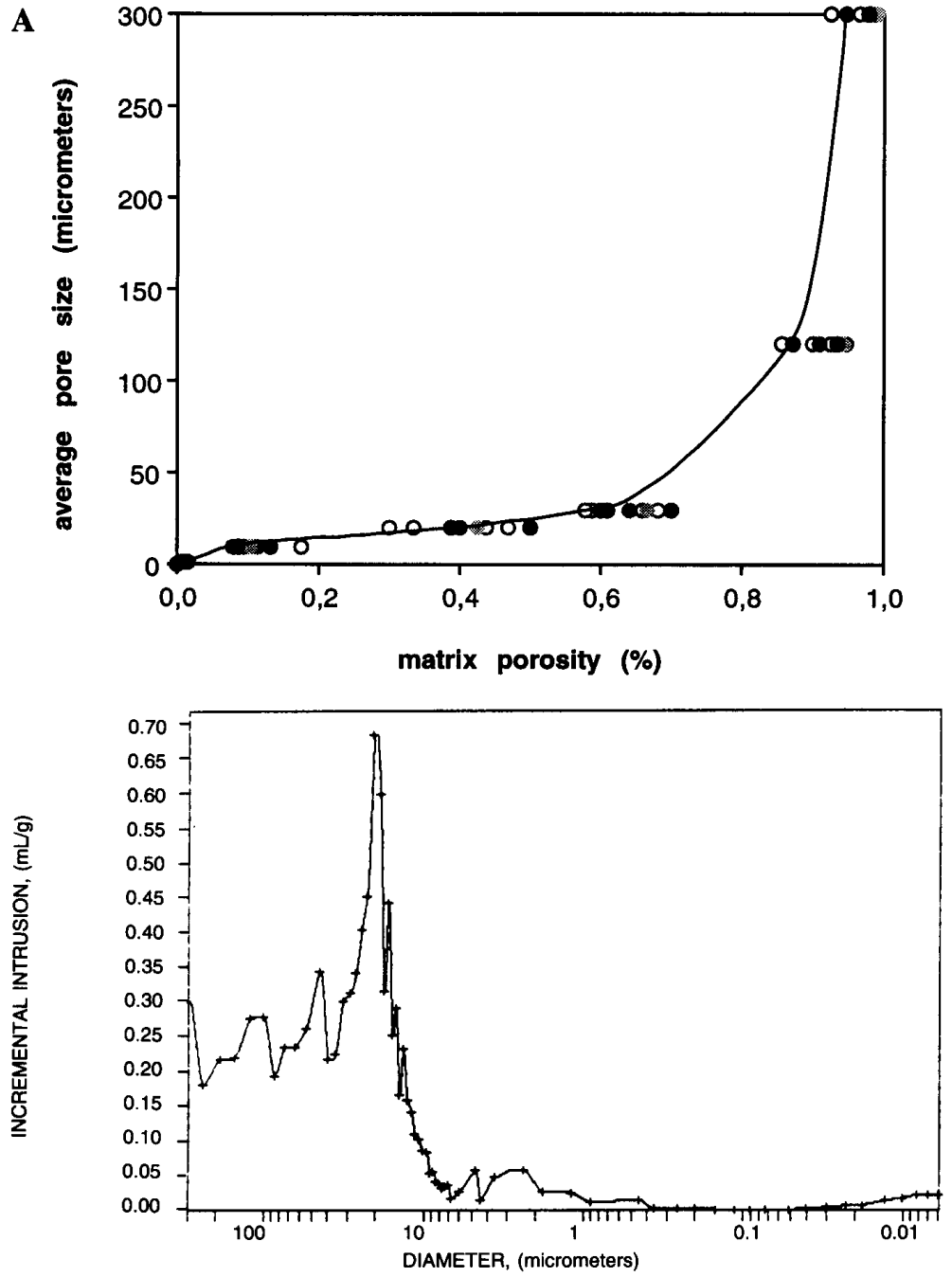

FIG. 4. **(A)** Matrix porosity of the PHPMA hydrogel as a function of pore size distribution. **(B)** Pore-size distribution as a function of the intruded volume of mercury into the hydrogel.

bridge between the transected spinal stumps (Fig. 5A). The hydrogel had merged with the cut surface of the spinal segments, delimiting a smooth and uniform interface, reestablishing the anatomical continuity of the tissue. The hydrogel showed a more compact structure made of polymer microspheres including various tissue elements that filled the entire porous network (Fig. 5B). Examination of the internal structure of the hydrogel matrix showed that the polymer network was invaded by tissue elements that had migrated from the adjacent host spinal tissue; thus cells, newly formed biological matrices, mostly made of tightly packed collagen fibers, and blood vessels were found within the porous network of the hydrogel implant (Fig. 5B–5D). There was no evidence of degradation of the structure of the PHPMA hydrogel when compared to the nonimplanted gel (see Fig. 3A). At high magnification, blood vessels were found to have grown within the space of the polymer network in contact to the microspheres and collagen matrices (Fig. 5C), and host tissue cells sent processes into the pores and around the polymer microspheres of the hydrogel (Fig. 5D), following the topography of the polymer surface network as also seen by TEM. At higher magnification, it could be seen that the microspheres were joined together by elastic fibrinogranular material, while the surface of the spheres showed the presence of deposited globular materials (Fig. 5E). Fibers that could be regenerating axons, were seen coursing onto the surface of the microspheres following the curvature of the polymer microsphere's topography of the hydrogel network (Fig. 5E).

Electron microscopic examination of the rostral spinal cord adjacent to the implantation site containing the polymer implant revealed myelinated axons with neurofilaments surrounded by glial cells with normal ultrastructural appearance (Fig. 6A). Figure 6B–6E shows the morphological appearance of the implantation site containing the PHPMA hydrogel implant. This region showed the reparative tissue which had formed within the polymer implant and the complex relationships between the polymer microspheres and the host tissue. The reparative tissue consistently showed cells and arrays of collagen fibers within the spaces between microspheres. Hence, cells that migrated into the porous structure of the PHPMA hydrogel gave rise to tissue that was moulded on the microgeometry of the surface of the polymer network by sending cytoplasmic expansions between the polymer microspheres (Fig. 6C and 6D). An examination of selected ultra thin sections showed that the glial cells infiltrated the polymer and sent pseudopode-like processes into the deepest portions of the gel, forming cell bridges between the polymer particles (Fig. 6D). Horn-like extensions of dark astrocytes (Fig. 6E) were also clearly seen extending towards a closely positioned particle. A space of 1–2 μm surrounding the polymer particle was constantly observed and which, most likely, was caused by the dehydration process during the preparation of the tissue with the gel implant. TEM observations showed consistently that the cytoplasmic components and the nucleus of the cells presented a normal ultrastructure. Blood vessels could be seen in the area of the gel implant in contact with polymer microspheres of the hydrogel implant, showing a normal structure (Fig. 6F). Demyelinated and myelinated axons were seen through the area of the hydrogel implant in contact with the polymer substrate, either along a longitudinal on transverse plane. In some instances, neuronal cell bodies were also seen sending an axon that terminated in a growth cone (Fig. 6G). In some areas of the implantation site of the spinal cord, a process of myelination could be seen; axons were surrounded by either thin or thick myelin sheaths. Nonmyelinated axons were sheathed by the cytoplasm of Schwann cells or astrocytic processes (Fig. 6H).

Implantation into the Cortex of P17 Rats: Immunocytochemistry Study

All brains contained hydrogel implants that were well attached to the surrounding host cerebral cortical tissue. Examples of gels in two of the brains are shown in Figure 7A and 7B. There was an increase in laminin immunoreactivity in some areas where the implant was attached to host neural tissue (arrows in Fig. 7A), but in other interface regions the laminin immunoreactivity was low (asterisks in Fig. 7A). An increase in GFAP immunoreactivity was seen in host cortex immediately surrounding the hydrogel implants (Figs. 7B and C and 10B and D). Note the absence of a glial scar around the entire perimeter of the implants.

Seven weeks after implantation, gels contained many laminin-positive profiles (Fig. 7A) and large numbers of infiltrating GFAP-positive astrocytes (Figs. 7B and 10B and D). Astrocytes and extracellular matrices were widely distributed throughout the gels in two cases, however, in the third animal laminin+ profiles were seen in less than half of the gels. A GFAP immunoreacted section from this gel is shown in Figure 7C, which show astrocytes located only in the medial and ventral parts of the implant. Some of these

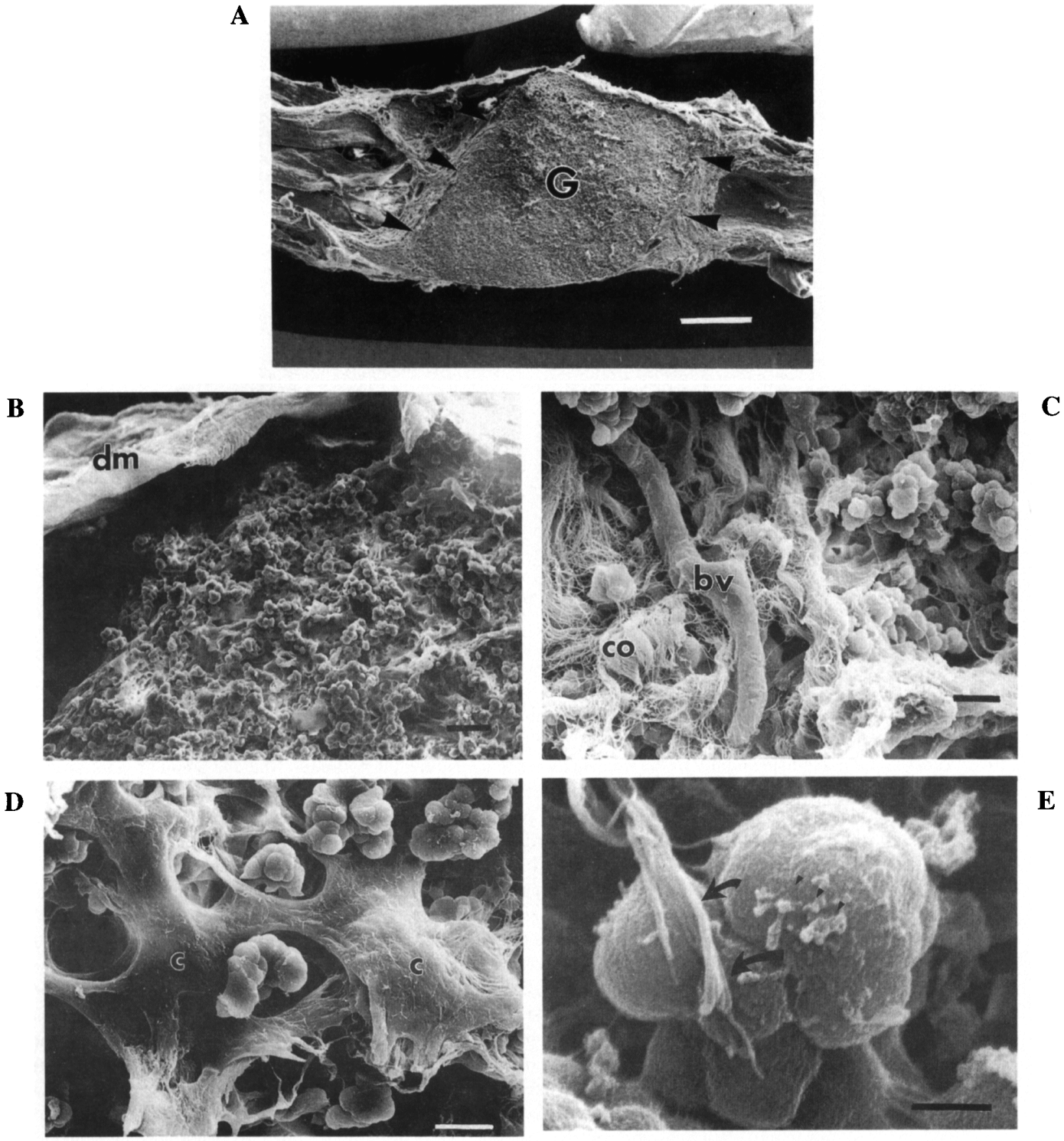

FIG. 5. SEM micrographs of the PHPMA hydrogel 5 months after implantation into the transected rat spinal cord. **(A),** low magnification microphotograph showing the hydrogel implant **(G)** that has merged with the two separated cut surface of the spinal cord, reconstituting the physical continuity of the cord. The arrowheads slow the interface between the polymer gel and the spinal cord. Note the cavitations in the adjacent neural tissue as a result of the transection injury. **(B)** shows the appearance of a hydrogel which has been infiltrated throughout the polymer network by host tissue (dm, dura matter). At higher magnification, blood vessels (bv) and associated collagen fibers (co) could be seen into the internal structure of the hydrogel **(C)**, and cells (c) were found to have sent pseudopod-like processes within the pores of the gel **(D)**. **(E)** shows fasciculated fibers resembling axons that were seen coursing along the surface of the polymer microspheres (arrows). Extracellular materials were seen at the surface of the polymer as shown by arrowheads in **(E)**. Scale bars: **(A)** = 500 μm; **(B)** = 20 μm; **(C–D)** = 10 μm; E = μm.

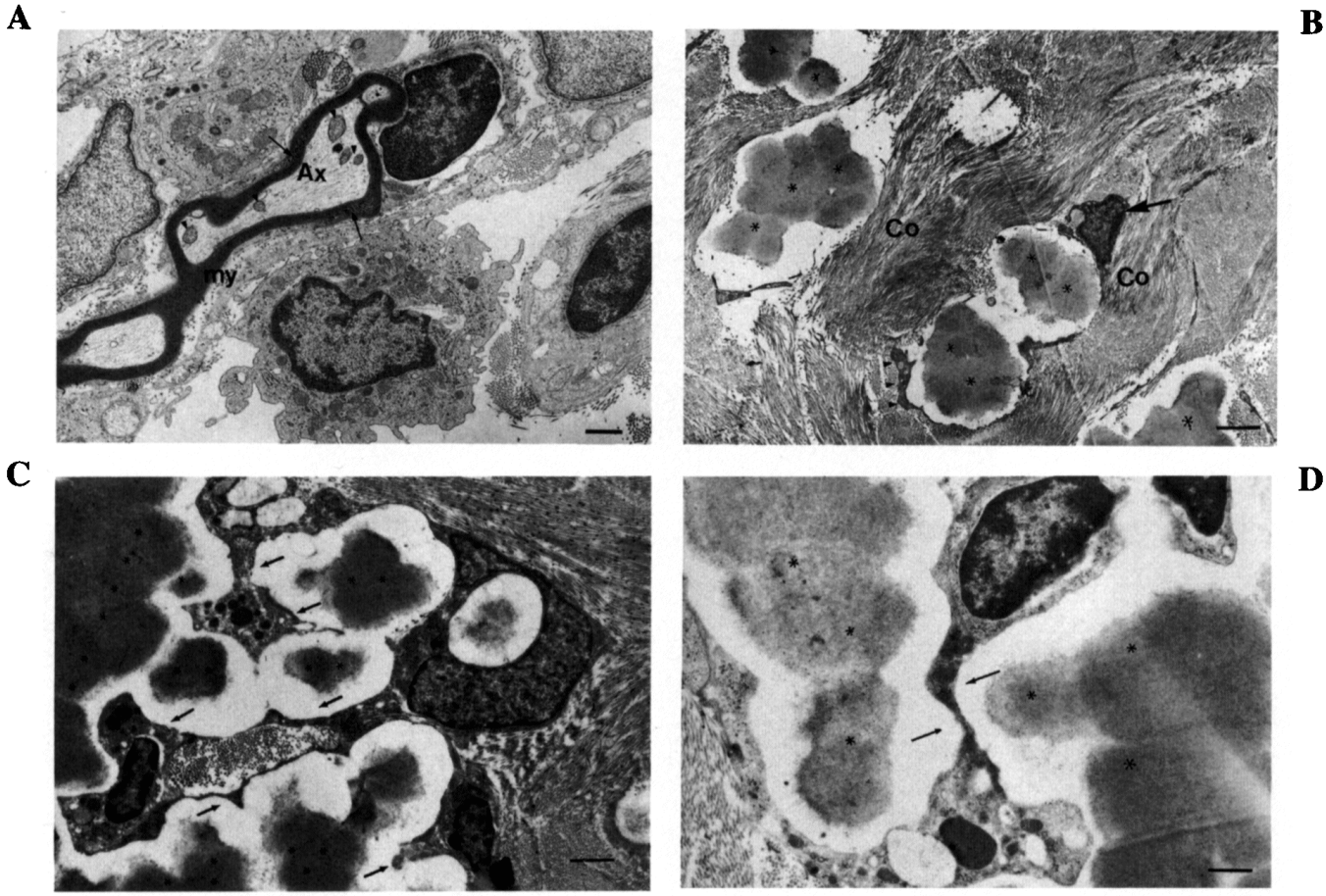

FIG. 6. TEM of longitudinal sections through the implantation site of the spinal cord containing the PHPMA hydrogel, 5-month after transection. **(A)** shows intact CNS-type myelin sheets (my) containing axons (Ax) and mitochondria (arrowheads) in the immediate vicinity of the implantation site containing the hydrogel. Note the Schmidt–Lantermann cleft (arrows). **(B)** shows tightly packed collagen fibres in three different orientations (longitudinal, oblique and perpendicular to the plane of the section) that surround the polymer microspheres of the hydrogel (asterisks). Note one cell (arrow) and cell processes (arrowhead) in direct contact to the polymer. **(C)** shows cells that have sent cytoplasmic expansions (arrows) between polymer microspheres (asterisks), following the microgeometry profile of the polymer surface as shown by the arrows. Note in the upper part of the figure a cross-shape cytoplasmic expansion emanating from one cell that has interdigited with four polymer microspheres. **(D)** and **(E)** show examples of two cells that have sent a thin long cytoplasmic process **(D,** arrows) and two horn-like extensions **(E,** arrows) of a dark astrocyte extending between microspheres clusters (asterisks). **(F)** cross-section of a small blood vessel that has grown into the polymer gel (asterisks) and which is surrounded by a basement membrane. **(G)** photomontage of series of longitudinal sections at the interface between the gel and the host tissue, showing a neuron with an axon (large arrowheads) that has grown along polymer particles of the gel (asterisks) and that terminate by a growth cone (small arrowheads at the right corner of the lower part of the figure). The small arrows show collagen fibers and the small arrowheads in the upper part of the figure indicate a dendritic contact. **(H)** shows various stages in the formation of myelin sheath about axons at the level of the implantation area;; there are axons with thick myelin sheats (large arrows) and other axons surrounded by a cell, presumptively a Schwann cell (Nu, Schwann cell nucleus); the small arrowheads show an external mesaxon. Scale bars: **(A), (D), (H)** = 1 μm; **(B), (C), (F), (G)** = 2 μm; **(E)** = 500 nm.

process-bearing GFAP-positive astrocytes are shown in higher magnification in Figure 7D. Gels also contained many S100-positive cellular profiles; the level of immunostaining for this antigen was most intense in regions of the implant containing GFAP and laminin immunoreactivity. Laminin-positive matrices deposits were clearly associated with the porous polymer network of the hydrogel (Fig. 7E) and with blood vessels that had grown into the implants (arrows in Fig. 7F).

All three gels contained regrown axons that were located in regions that contained infiltrated cells and laminin matrix deposits. These regenerating axons could be visualized using antibodies to either GAP-43

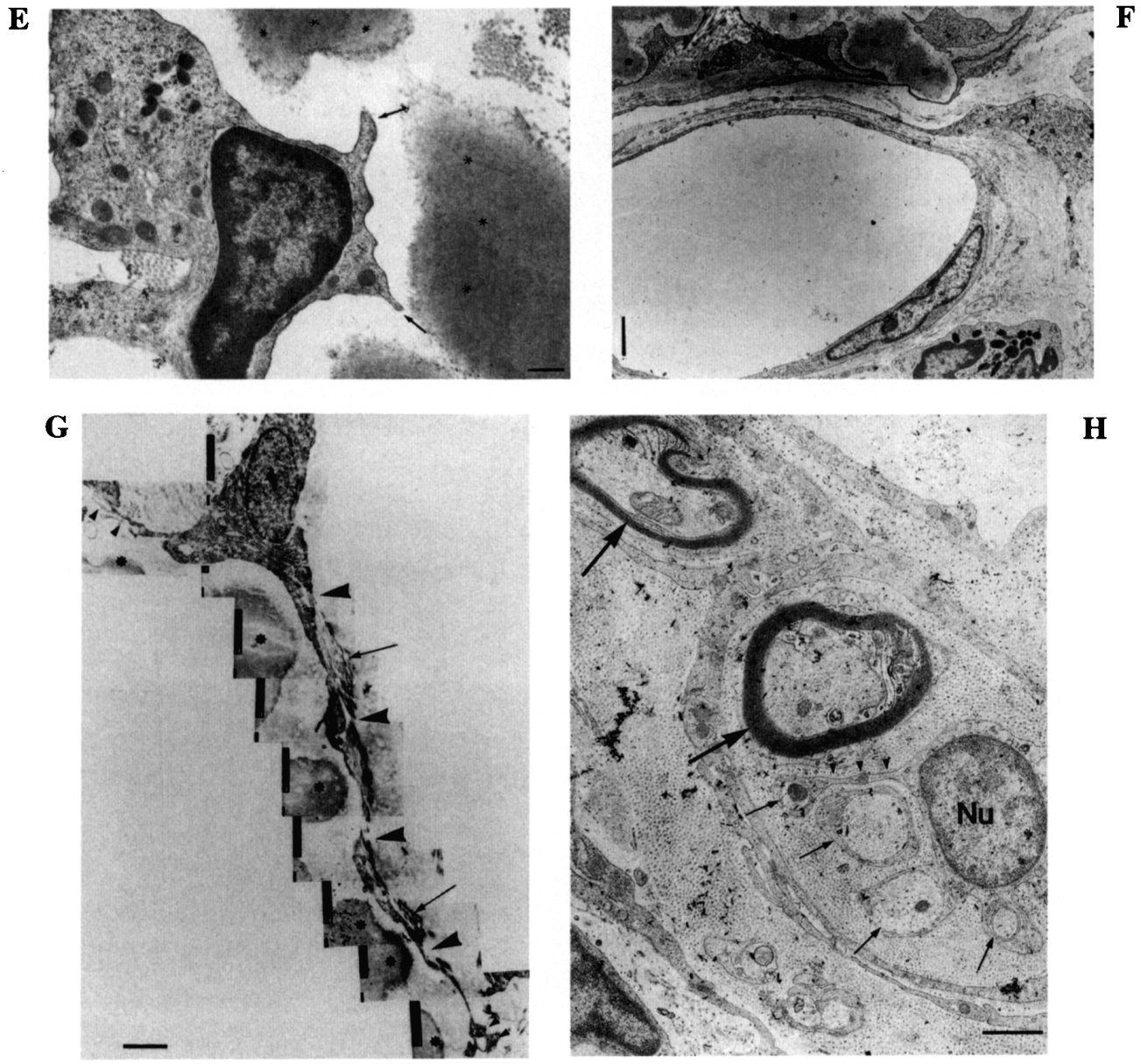

FIG. 6. (*continued*)

(Fig. 7G) or RT-97 (Fig. 7H). Macrophages were also seen in the gels, often in regions where the polymer matrix was less dense or fragmented (Fig. 7I). It is possible that some of this gel fragmentation was a result of tissue processing artefact. However, the presence of macrophages may indicate that there was some ongoing reorganization of parts of the matrix *in vivo.*

Implantation into the Cortex of P21 Rats: TMA^+ Diffusion Parameters in the PHPMA Hydrogel Implant

Diffusion measurements were performed in hydrogels before and after implantation and compared with those obtained in the host brain distant from the implant. Examples of such diffusion curves are shown in Figure 8. The mean values of volume fraction (α) and tortuosity (λ) in host cortex were 0.21 ± 0.004 and 1.60 ± 0.019, respectively (mean ± SE, n = 24); that is, they were not different from those described in intact brain,[38] while in the PHPMA hydrogel α = 0.80 ± 0.013 and λ = 1.13 ± 0.008 (n = 14), suggesting that the pore size of the gel structure is much larger than that of the nervous tissue and with less hindrance for diffusion. At a postimplantation time of 34–69 days, the volume fraction in hydrogels signifi-

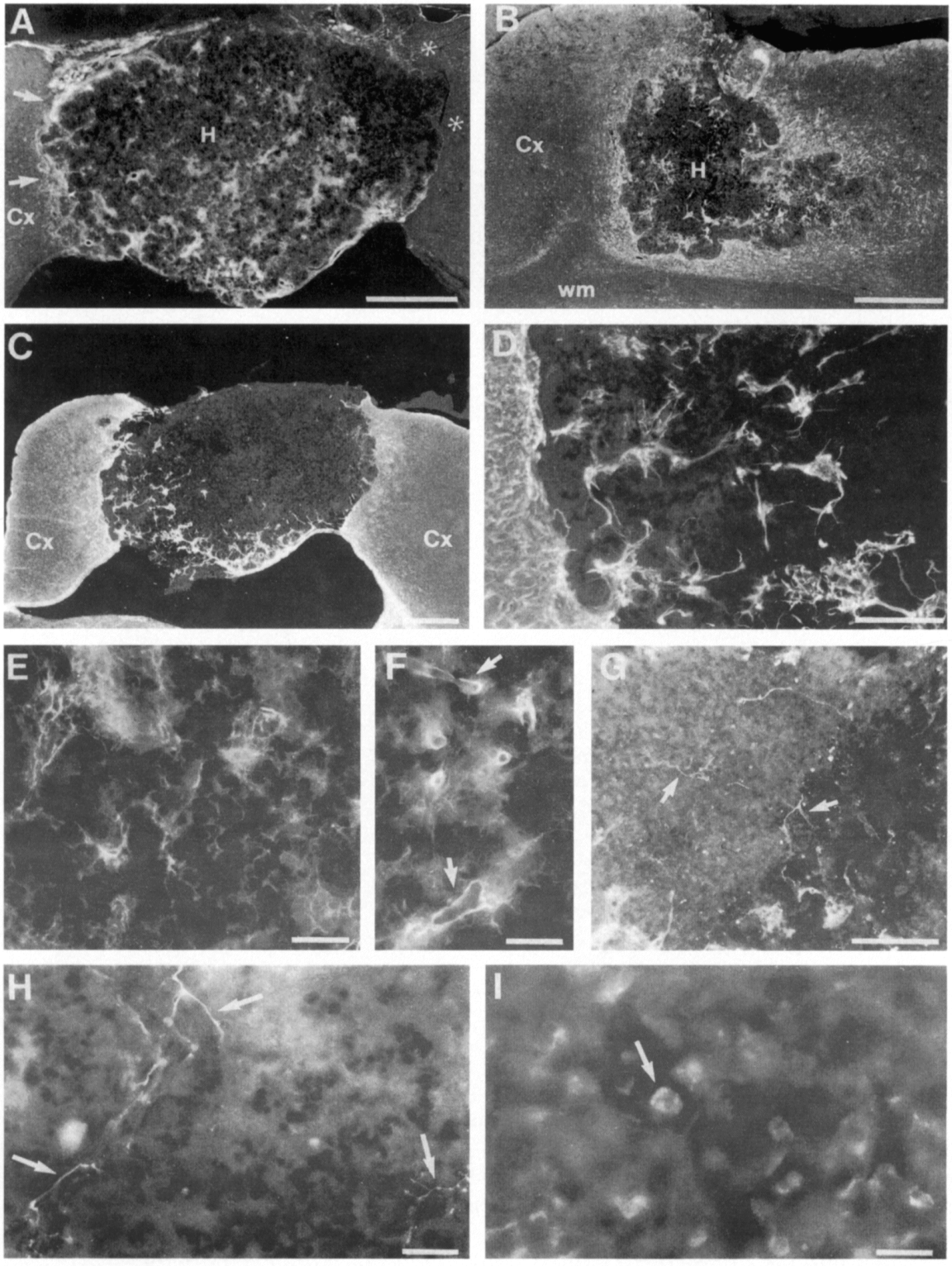

FIG. 7. Fluorescence photomicrographs of immunostained coronal sections of hydrogels implanted into frontal cortex lesion cavities. **(A)** laminin$^+$ matrix within an implanted hydrogel **(H)**. Increased laminin immunoreactivity was seen in some (arrows) but not all (asterisks) parts of the brain/gel interface. **(B)** large numbers of the host GFAP$^+$ astrocytes within a hydrogel (H). Note increased astrocytic reactivity in the cortex (Cx) surrounding the implant. **(C)** a gel only partially colonized by astrocytes. **(D)** higher power view of part of the gel shown in C. Host cortex is to the left. Note large numbers of GFAP$^+$ process-bearing astrocytes within the polymer gel. **(E–F)** Laminin immunoreactivity within implanted hydrogels. The extracellular matrix molecules were scattered throughout the porous network of the hydrogels **(E)** or were associated with blood vessels [arrows in **(F)**]. **(G)** GAP-43$^+$ axons (arrows) within a hydrogel. **H**, RT-97$^+$ axons (arrows) that grew back into the implanted gel. **(I)** ED1+ macrophages (arrow) inside a hydrogel. Wm, white matter. Scale bars: **(A–C)** = 500 μm; D, **(G)** = 200 μm; **(E, F, H)** = 50 μm; **(I)** = 25 μm.

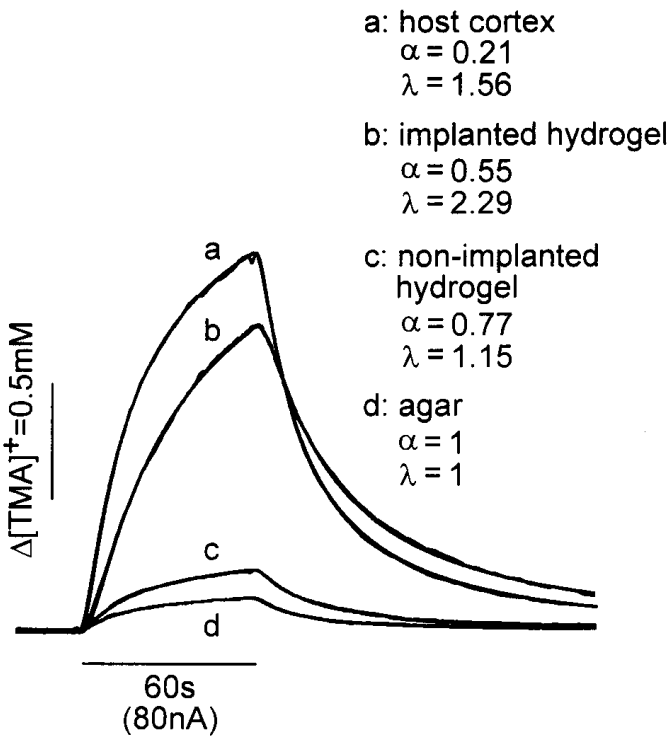

FIG. 8. Examples of TMA^+ diffusion curves obtained in host cortex **(a)**, in implanted gel **(b)**, in hydrogel before implantation **(c)**, and in agar **(d)**. The concentration scale is linear and the theoretical diffusion curve is superimposed on each experimental curve. The higher the curve the smaller the volume fraction. The rise and decay time of the curve is slower in the implanted gel because of the increased tortuosity in less permissive tissue.

cantly decreased to a value of 0.49 ± 0.038, while tortuosity significantly increased to a value of 2.17 ± 0.041 (n = 36), apparently due to ingrowth of cells and fibers into the gel implant. Both α and λ values in the hydrogels were therefore significantly higher than those in the host cortex (Table 1 and Fig. 8). Table 1 further shows that there was a similar uptake k' in implanted hydrogel as seen in the host cortex, suggesting the presence of cellular uptake in the implanted hydrogel. Figure 9 shows two-dimensional isoconcentration plots of TMA^+ concentration in the host cortex, in the implanted hydrogel infiltrated with brain cells and in the nonimplanted hydrogel. Isoconcentration plots were calculated after 60 sec of iontophoretic application of TMA^+ using mean values of α, λ, and k' (Fig. 9). It is obvious that the sphere of isoconcentration circles in which a given TMA^+ concentration (0.1–1.0 mM TMA^+) was reached was larger in host cortex than in the implanted hydrogel. The larger sphere of the host cortex indicates that at a given distance from the point source, TMA^+ concentration reaches higher values in cortex than in implanted hy-

TABLE 1. MEAN VALUES (MEAN ± SE) OF ECS DIFFUSION PARAMETERS IN HOST CORTEX, IN IMPLANTED HYDROGEL AND NONIMPLANTED HYDROGEL

	n	α	λ	κ' ($\times 10^{-3}$ s^{-1})
Host cortex	24	0.21 ± 0.004	1.60 ± 0.019	4.71 ± 0.358
Implanted hydrogel	36	0.49 ± 0.038	2.17 ± 0.041	6.65 ± 0.826
		$p_1 < 0.0001$	$p_1 < 0.0001$	$p_1 = 0.07$
Nonimplanted hydrogel	14	0.80 ± 0.013	1.13 ± 0.008	0
		$p_2 < 0.0001$	$p_2 < 0.0001$	$p_2 < 0.0001$

p_1, = statistical significance of difference as compared to host cortex; and p_2 = statistical significance of difference as compared to implanted hydrogel.

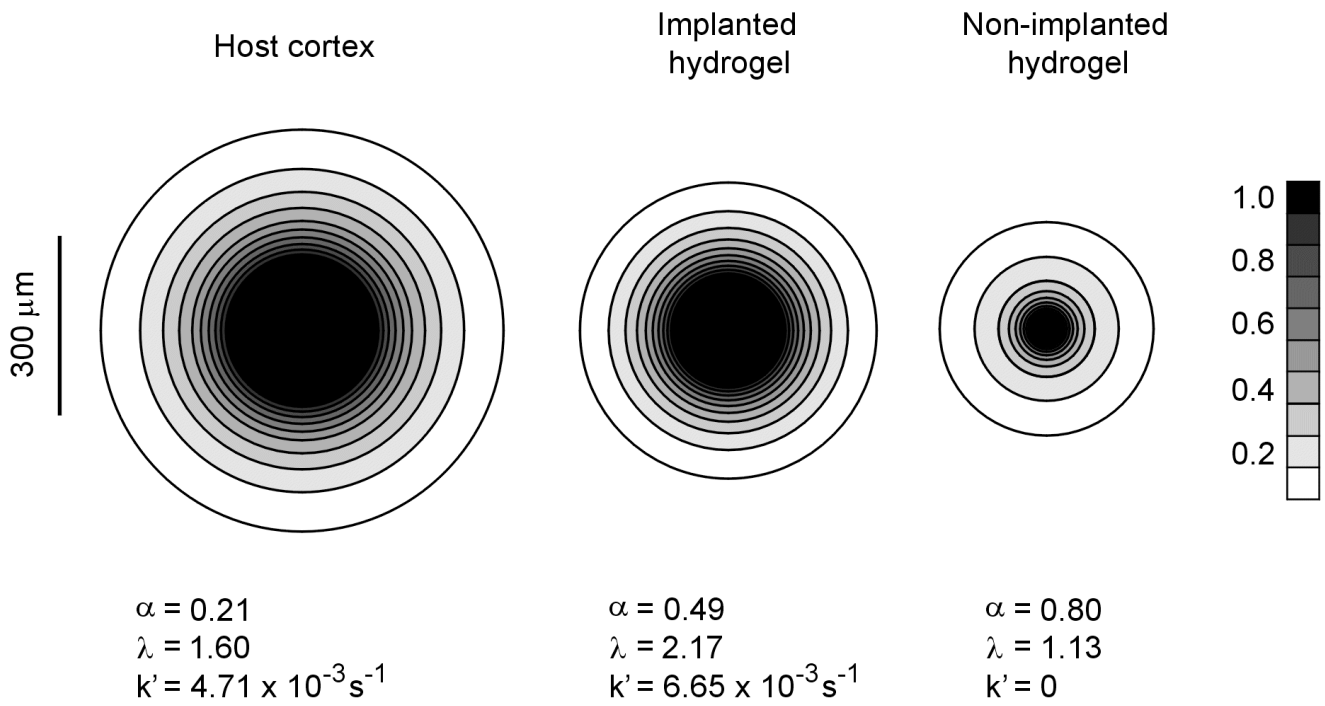

FIG. 9. Two-dimensional isoconcentration plots of TMA^+ concentration in host cortex, implanted hydrogels, and nonimplanted hydrogels after 60 sec of iontophoretic application of TMA^+. Grey densities represent different concentrations of TMA^+ from 0.1 to 1.0 mM. Isoconcentration plots were calculated using mean values of diffusion parameters obtained from host cortex, implanted hydrogels, and nonimplanted hydrogels. The iontophoretic pipette served as a point source of TMA^+. The bigger the sphere, the more restricted the diffusion of TMA^+ in that region.

drogel due to the smaller ECS volume in nervous tissue and the difference is even larger when compared to nonimplanted hydrogel. However, as shown in Figure 8, the TMA^+ diffusion curve is rising faster in the host cortex than in implanted hydrogel with more diffusion barriers, as shown by an increase in tortuosity.

Histological sections of the brain cortex containing the hydrogel were either stained with cresyl violet or immunostained for GFAP, and microelectrode tracks were identified to compare diffusion parameters and morphological data. An example of such analysis is presented in Figure 10. There was GFAP staining in the hydrogels and in adjacent host cortex, the level of GFAP expression decreasing with increasing distance from the implant (Fig. 10B and D). Gels contained different levels of GFAP staining intensity, and this correlated with differences in diffusion parameter values of the implants. The values of α and λ obtained from hydrogels displaying extensive infiltration by astrocytes and a high level of astrogliosis in the adjacent host brain (Fig. 10A, B, C, and D) were significantly different from the values seen in gels with poor astrocytic infiltration (Fig. 10E and F). The values in gels with poor astrocytic infiltration were more similar to those observed in the nonimplanted polymer (Table 1).

DISCUSSION

The primary goal of this study was to assess the ability of the PHPMA hydrogel to induce the formation of a reparative tissue and promote axonal regeneration after implantation into lesion cavities of the rat spinal cord or cerebral cortex. A large tissue defect was surgically created, thus the response of host CNS tissue was the result of the influence of the hydrogel on the wound-healing process. In normal conditions, this response results in the formation of a scar that seals off the lesion and impedes axon regeneration. The purpose of implanting the PHPMA hydrogel was to provide a stable three-dimensional substrate that facilitated tissue replacement, encouraged axon regrowth and reduced scar formation. Tissue infiltration into the gels occurred and was assessed using immunocytochemical and ultrastructural techniques. In addition, tis-

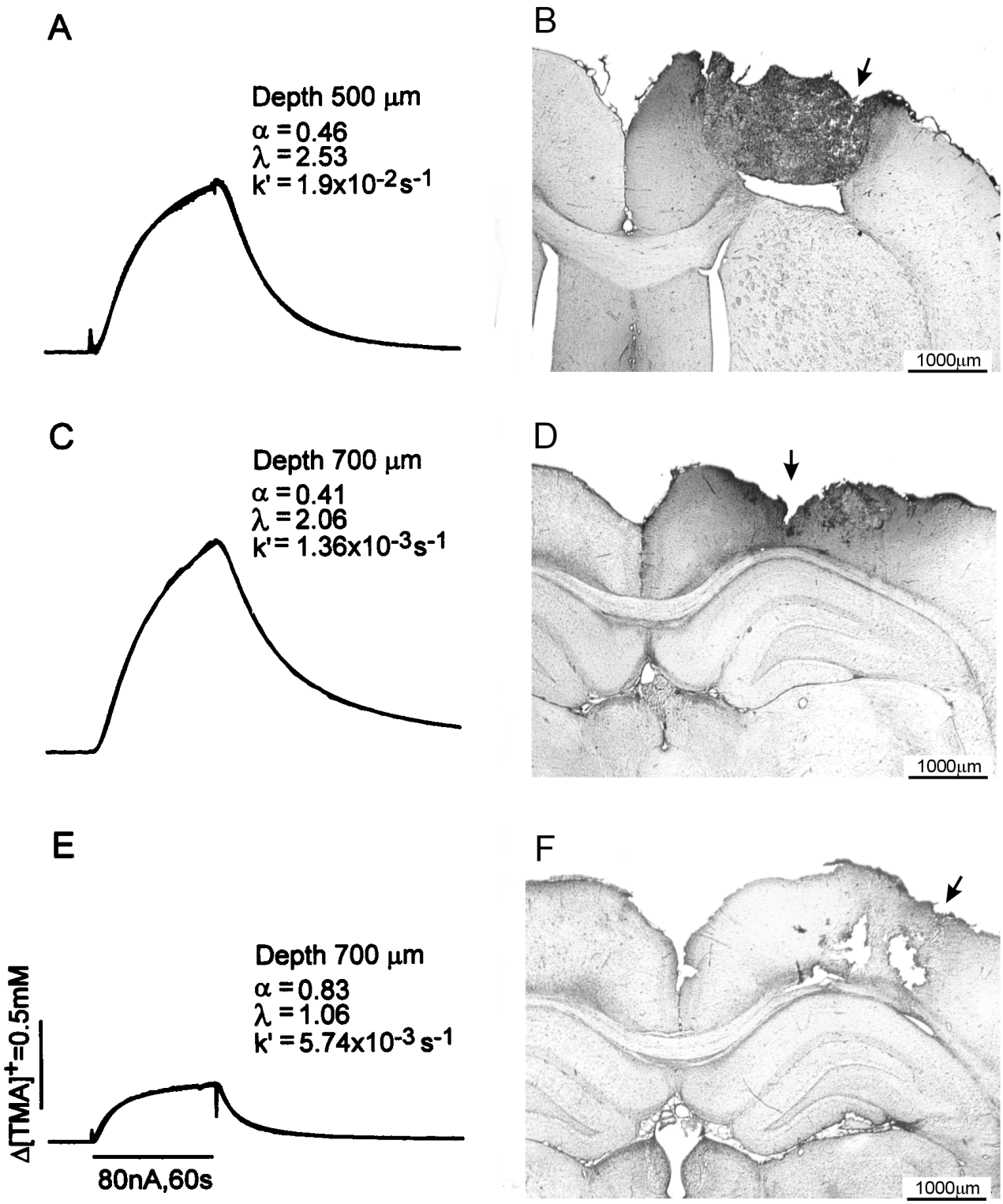

FIG. 10. TMA^+ diffusion curves with values of α, λ, and k' and corresponding photomicrographs of coronal sections immunostained for GFAP showing the location of electrode tracks in implanted hydrogels. **(A, B)** Animal 69 days postimplantation; diffusion curve recorded from a depth of 500 μm from the cortical surface. **(C, D)** Animal 65 days postimplantation; diffusion curve recorded from a depth of 700 μm from the cortical surface. **(E, F)** Animal 44 days post implantation; diffusion curve recorded from a depth of 70 μm from the cortical surface. Note the correlation of high **(B, D)** and low **(F)** levels of GFAP expression with differences in diffusion parameter values.

sue ingrowth was correlated with *in vivo* physiological changes in diffusion parameters within the PHPMA hydrogel. This study confirms previous studies that the PHPMA hydrogel can effectively bridge tissue defects in the CNS, with recruitment of cells and blood vessels from host tissue contacting the hydrogel surface, and axonal regrowth into and through the polymer matrix.[4,30] In addition, this result provides new insight into the relationship between the structure units of the PHPMA hydrogel and the reparative neural tissue at the ultrastructural and electrophysiological level. We have previously shown that the PHPMA gel exhibits mechanical behavior similar to rat neural tissue, and therefore minimal mechanical irritation is produced by the presence of hydrogel.[4] This is an important property that explains the mechanical integrity of the gel upon implantation and its integration to the neural tissue. Indeed, studies have shown that if this does not occur the hydrogel implant becomes encapsulated without tissue integration.[26] This is confirmed in the present study at the ultrastructural level. The matching between the mechanical behavior of the hydrogel and the soft neural tissue facilitates tissue organization in the time scale required for tissue ingrowth, organization, and axonal regeneration.

The *in vivo* TMA^+ diffusion studies indicate that there is a resemblance between the PHPMA hydrogel and developing neural tissue, which has relatively large extracellular spaces, represented by a significant volume fraction.[37,38] In early postnatal days, the TMA^+ diffusion parameters in rat cortex and corpus callosum are significantly different from those in adults. The extracellular space volume fraction α in a newborn rat is more than twice as large (about 0.45) as it is in adult rat brain (about 0.20).[37] Recently, a similar decrease in α and λ was demonstrated in the developing rat spinal cord gray and white matter.[39] On the basis of the similarity between the volume fraction (space available for diffusion) of the developing rat brain and the PHPMA hydrogel, we can speculate that these gel properties may facilitate the diffusion of the various growth factors that are secreted by the activated cells such as astrocytes in a similar way as may occur in the developing brain. This could explain the rapid tissue invasion, principally of glial origin, within the porous structure of the gel.

The decrease of the extracellular space volume fraction of the hydrogel 6–10 weeks after implantation (from $\alpha = 0.80$ to $\alpha = 0.49$) is explained by the invasion of glial cells and the outgrowth of regenerating axons and blood vessels throughout the hydrogel implant. However, α still remains larger than in adult rat brain, although similar to the value found in the newborn rat brain. The increase of tortuosity at this time point postimplantation may be related to the presence of large numbers of GFAP-positive astrocytes. Increased tortuosity were also observed in neural tissue that showed astrogliosis[40,41] and in astrogliotic tissue around cortical stab wounds.[42] Hypertrophied astrocytic processes, as well as a variety of adhesion molecules, molecules of extracellular matrix, and cytokines produced by reactive astrocytes may impose additional diffusional barriers and lead to an increase in λ.

The PHPMA hydrogel has several properties that are important for tissue repair in the context of the wound-healing response initiated by the surgical trauma of implantation. First, the hydrogel acts as a space-filling material and as a scaffold-builder for tissue formation/remodeling during the healing process. Host cells migrate into the gels and the matrix supports angiogenesis. In addition, biological extracellular matrices produced by activated cells were deposited onto and within the polymer network as seen using anti-laminin immunocytochemistry and at the ultrastructural level. Hence, laminin, which has been shown to favor axonal growth *in vitro* and *in vivo*,[43] was found widely distributed throughout the hydrogel 7 weeks after implantation in the brain. In the spinal cord, collagen, which is naturally produced after injury by epithelio-mesenchymal interactions, was found to form a loosely arranged network throughout the polymer microspheres of the hydrogel. Such organization facilitated cells and blood vessel infiltration into the lesion site. A main component of ingrown tissue within the hydrogel implant is the astrocytes and their processes as shown by GFAP immunostaining. These cells display considerable plasticity and by infiltrating their processes within the hydrogel, they establish a sustaining cell matrix from the interface toward the center of the implant with a topology that is imposed by the microgeometry of the polymer network. In addition, reactive astrocytes may play a major role in the function of the polymer implant because these cells are known to support, in certain conditions, axonal growth by producing neural cell adhesion molecules and by secreting growth factors and cytokines that support survival and axonal regeneration in injured CNS.[30,44–49] In infiltration of astrocytes within the polymer hydrogel provides a glial environment that contributes to the maintenance of structure and homeostasis in repaired tissue. In addition, this glial tissue en-

vironment is permissive to axonal regeneration as shown in the present study by immunolabeling of regenerating axons in lesion of the frontal cortex using GAP-43, a marker of neuronal development and plasticity,[50] and by ultrastructural techniques showing the presence of unmyelinated axons in the hydrogel structure in the lesioned spinal cord. The presence of myelinated axons in the hydrogel structure was indicative of processes of myelination in the implantation area. The myelination process may be due to either by Schwann cells that had migrated into the lesion site or by oligodendrocytes, and has been regarded as a normal physiological response to injury.[51] Proliferation and migration of endothelial, epithelial, and connective tissue cells also contribute to tissue growth as a result of secretion of cytokines by blood-borne monocytes and resident glia.[52] According to the measured diffusion characteristics, the hydrogel acts also as a reservoir for the sequestering of the various bioactive factors that are secreted by the host tissue for neuritic growth and cell survival.[53]

Two parameters are important for the functionality of the PHPMA hydrogel; the structural characteristics of the hydrogel and the type and severity of the CNS lesion. Mercury porosimetry and diffusion measurement show that the structure of the PHPMA hydrogel is made up of a large void volume associated with an extensive network of interconnected open pores. Complementary methods to measure meso- and micropore range have shown that the porous structure of the PHPMA hydrogel encompasses a large range of porosity (unpublished data). This porous structure forms a scaffold for cell infiltration, tissue growth, and organization, and allows the formation of a reparative tissue within the PHPMA hydrogel. This is the result of three levels of interaction with the host tissue. At the macroscopic level, the polymer hydrogel moulds the lesion cavity and adheres to the host tissue, ensuring the complete sealing of the tissue defect with the formation of a permissive interface with the host tissue. The level of pore size distribution and the degree of pore interconnection control and gives polarity to the ingrowing tissue cells, allowing their organization into a spatial arrangement. Finally, the surface of the polymer network controls the molecular interactions with cell membranes and biological fluids. However, the biofunctionality of the polymer hydrogel is also dependent upon the type and severity of the lesion. Hence, the mode of severance of the spinal cord is important because the final appearance of the lesion depends on the degree of the initial trauma; the integration of the PHPMA hydrogel into the injured spinal cord is facilitated when the double transection is made sharp and clean of cell debris, blood and mesenchymal tissue, without causing a secondary trauma of the spinal stumps.[54] Thus, the formation of a reparative tissue within the hydrogel implant depends on the histopathological history of the lesion. In such conditions, scar tissue is not seen and the surface of the lesions can form a clean interface with the hydrogel, facilitating the infiltration of cells within the polymer hydrogel. The feasibility of achieving some degree of tissue repair implies that the quality of the lesion/implantation surgical procedure is important for enhancing wound healing and tissue repair. As shown in previous studies, this is indicative of a dynamic balance between necrotic and reparative processes in the injured spinal cord.[52] Although the experimental transection model of spinal cord is different from most human spinal cord injuries that are mainly incomplete and result from a compression/decompression mechanism, the above considerations are important in terms of a reparative surgical procedure to promote tissue repair and axonal regeneration. Hence, the implantation of PHPMA hydrogel into a cystic cavity of a chronic lesion of the rat spinal cord produced by compression, induces an histopathological reaction that promotes tissue ingrowth and axon regeneration within the hydrogel implant from the surrounding spared spinal cord tissue.[55]

The success of tissue regeneration depends also on the mechanical integrity of the polymer matrix and on the degree of tissue ingrowth and the quality of tissue organization. In this respect, the microgeometry of the surface of the network of polymers, the pore size distribution and the degree of pore interconnection in the hydrogel matrix, and the viscoelastic properties are important design characteristics of the gel. Tissue ingrowth may be manipulated by adding function chemical or biological groups to the polymer network. The rational design of hydrogels with bioactive surface agents for neural tissue repair stems from advances in understanding the role of extracellular matrix molecules in regulating cell adhesion, growth, and differentiation during tissue morphogenesis, tissue remodelling, and repair. For example, hydrogels containing glucosamine residues, acetyl derivatives, or RGD sequences have been shown to support neural cell adhesion and growth *in vitro* in absence of non neuronal cells and *in vivo*.[30,56,57]

To date, for promoting axon regeneration in the injured adult spinal cord current therapeutic approaches

include the use of antibodies against oligodendroglia inhibitory proteins, peripheral nerve bridge grafts, multiple grafts of embryonic-type tissue, chemical bridges, artificial bridges (collagen tubes, polyglycolic acid, matrigel, nitrocellulose), and trophic factor delivery systems.[15] The use of polymer hydrogels tailored to exhibit morphogenetic autonomy upon transplantation represent an additional approach that has potential therapeutic applications for neural tissue reconstruction and repair.[58,59] Restoration of tissue and potential functional recovery in the adult mammalian CNS depends therefore on the possibility of inducing astrocytic, vascular, and mesenchymal tissue reconstitution of the injured defect and the creation of a permissive tissue bridge across the injury site.

ACKNOWLEDGMENTS

Eva Syková was supported by GACR Grant Nos. 307/96/K226, 305/99/0655, 309/99/0657, and VS 99-130, and Alan Harvey was supported by the Australian NHMRC (Grant No. 970098).

REFERENCES

1. Richardson, P.M., McGuinness, U.M., and Aguayo, A.J. Axons from the CNS neurones regenerate into PNS grafts. Nature **284,** 264, 1980.
2. Davies, S.J.A., Field, P.M., and Raissman, G. Embryonic tissue induces growth of adult axons from myelinated fiber tracts. Exp. Neurol. **145,** 471, 1997.
3. Singer, M, Nordlander, R.H., and Egar, M. Axonal guidance during embryogenesis and regeneration in the spinal cord of the newt: The blueprint hypothesis of neuronal pathway patterning. J. Comp. Neurol. **185,** 1, 1979.
4. Woerly, S., Pinet, E., de Robertis, L., et al. Heterogeneous phpma hydrogels for tissue repair and axonal regeneration in the injured spinal cord. J. Biomat. Sci. Polymer Ed. **9,** 681, 1998.
5. Brockes, J.P. Amphibian limb Regeneration: Rebuilding a complex structure. Science **276,** 81, 1997.
6. Larner, A.J., Johnson, A.R., and Keynes, R.G. Regeneration in the vertebrate central nervous system: phylogeny, ontogeny and mechanisms. Biol. Rev. **70,** 597, 1995.
7. Simpson, S.B., and Duffy, M.T. The lizard spinal cord: A model system for the study of spinal cord injury and repair. Progress Brain Res. **103,** 229, 1994.
8. Arsanto, J.P., Komorowski, T.E., Dupin, F., et al. Formation of the peripheral nervous system during tail regeneration in urodele amphibians: Ultrastructural and immunocytochemical studies of the origin of the cells. J. Exp. Zool. **264,** 273, 1992.
9. Michel, M.E., and Reier, P.J. Axonal-ependymal associations during early regeneration of the transected spinal cord in Xenopus laevis tadpoles. J. Neurocytol. **8,** 529, 1979.
10. Prehn, R.T. Regeneration versus neoplastic growth. Carcinogenesis **18,** 1439, 1997.
11. Guth, L., Barrett, C.P., Donati, E.J., Anderson, F.D., Smith, M.V., and Lifson, M. Essentiality of a specific cellular terrain for growth of axons into a spinal cord lesion. Exp. Neurol. **88,** 1, 1985.
12. Beattie, M.S., Bresnahan, J.C., Komon, J., et al. Endogeneous repair after spinal cord contusion injuries in the rat. Exp. Neurol. **148,** 453, 1997.
13. Aubert, I., Ridet, J.L., and Gage, F.H. Regeneration in the adult mammalian CNS: Guided by development. Curr. Opin. Neurobiol. **5,** 625, 1995.
14. Stichel, C.C., and Müller, W.H. Experimental strategies to promote axonal regeneration after traumatic central nervous system injury. Progress Neurobiol. **56,** 119, 1998.
15. Olson, L. Regeneration in the adult central nervous system: experimental repair strategies. Nat. Med. **3,** 1329, 1997.
16. Marchand, R., and Woerly, S. Transected spinal cords grafted with in situ self-assembled collagen matrices. Neuroscience **36,** 45, 1990.
17. Spilker, M.H., Yannas, I.V., Hsu, H-P., Norregaard, T.V., Kostyk, S.K., and Spector, M. The effect of collagen-based implants on early healing of the adult rat spinal cord. Tissue Eng. **3,** 309, 1997.
18. Goldsmith, H.S., and de la Torre, J.C. Axonal regeneration after spinal cord transection and reconstruction. Brain Res. **589,** 217, 1992.
19. Bernstein, J.J., and Goldberg, W.J. Transplantation of cultured fetal spinal cord grafts, grown on a histocompatible substrate, into adult spinal cord. Brain Res. **377,** 403, 1986.
20. Paino, C.L., Fernandez-Valle, C., Bates, M.L., and Bunge, M.B. Regrowth of axons in lesioned adult rat spinal cord: promotion by implants of cultured. Schwann cells. J. Neurocytol. **23,** 433, 1994.

21. Schreyer, D.J., and Jones, E.G. Growth of corticospinal axons on prosthetic substrates introduced into the spinal cord of neonatal rats. Dev. Brain Res. **35,** 291, 1987.
22. Xu, X.M., Guénard, V., Kleitman, N., and Bunge, M.B. Axonal regeneration into Schwann cell-seeded guidance channels grafted into transected adult rat spinal cord. J. Comp. Neurol. **351,** 145, 1995.
23. Montgomery, C.T., Tenaglia, E.A., and Robson, J.A. Axonal growth into tubes implanted within lesions in the spinal cords of adult rats. Exp. Neurol. **137,** 277, 1996.
24. Harvey, A.R., Connor, A.M., Grounds, M.D., and Beilharz, M.W. The migration and intermixing of donor and host gila on nitrocellulose polymer implanted into cortical lesion cavities in adult mice and rats. Int. J. Dev. Neurosci. **11,** 569, 1993.
25. Shugens, Ch., Grandfils, Ch., Jerome, R., et al. Preparation of a macroporous biodegradable polylactide implant for neuronal transplantation. J. Biomed. Mat. Res. **29,** 1349, 1995.
26. Woerly, S., Marchand, R., and Lavallée, C. Intracerebral implantation of synthetic polymer/biopolymer matrix: A new perspective for brain repair. Biomaterials **11,** 97, 1990.
27. Woerly, S. Porous hydrogels for neural tissue engineering. In: Liu, D-M, Dixit, V., eds. Porous Materials for Tissue Engineering. Switzerland: Trans. Tech. Publications, 1997, p. 53.
28. Woerly, S, Ulbrich, K., Chytry, V., et al. Synthetic polymer matrices for neural cell transplantation. Cell Transpl. **2,** 229, 1993.
29. Plant, G.W., Harvey, A.R., and Chirila, T.V. Axonal growth within poly (2-hydroxyethyl methacrylate) sponges infiltrated with Schwann cells and implanted into the lesioned rat optic tract. Brain Res. **671,** 119, 1995.
30. Plant, G.W., Woerly, S., and Harvey, A.R. Hydrogels containing peptide or aminosugar sequences implanted into the rat brain: Influence on cellular migration and axonal growth. Exp. Neurol. **143,** 287, 1997.
31. Plant, G.W., Chirila, T.V., and Harvey, A.R. Implantation of collagen IV/poly (2-hydroxyethyl methacrylate) hydrogels containing schwann cells into the lesioned rat optic tract. Cell Transpl. **7,** 381, 1998.
32. Ratner, B.D., and Hoffman, A.S. Synthetic hydrogels for biomedical applications. In: Andrade, J.D., ed. Hydrogels for Medical and Related Applications. ACS Symp. Ser. **31,** 1976, p. 1.
33. Park, H., and Park, K. Hydrogels in Bioapplications. In: Ottenbrite, R.M., Huang, S.J., Park, K., eds. Hydrogels and Biodegradable Polymers for Bioapplications. ACS Symp. Series 627, Washington DC, 1996, p. 2.
34. Dumitriu, S., and Dumitriu-Medvichi, C. Hydrogel and general properties of biomaterials. In: Dumitriu, S., ed. Polymeric Biomaterials. New York: Marcel Dekker, Inc., 1994, p. 3.
35. Nicholson, C., and Phillips, J.M. Ion diffusion modified by tortuosity and volume fraction in the extracellular microenvironment of the rat cerebellum. J. Physiol. Lond. **321,** 225, 1981.
36. Syková, E., Svobodova, J., Polák, J. and Chvátal, A. Extracellular volume fraction and diffusion characteristics during progressive ischemia and terminal anoxia in the spinal cord of the rat. J. Cereb. Blood Flow Metab. **14,** 301, 1994.
37. Lehmenkühler, A., Syková, E., Svoboda, J., Zilles, K., and Nicholson, C. Extracellular space parameters in the rat neocortex and subcortical white matter during postnatal development determined by diffusion analysis. Neuroscience **55,** 339, 1993.
38. Vorisek and Syková, E. Evolution of anisotropic diffusion in the developing rat corpus callosum. J. Neurophysiol. **78,** 912, 1997.
39. Propoková, S., Vargová, L., and Syková, E. Heterogeneous and anistropic diffusion in the developing rat spinal cord. Neuroreport **8,** 3527, 1997.
40. Syková, E., Vargová, L., Propoková, S., and Simonová, Z. Glial swelling and astrogliosis produce diffusion barriers in the rat spinal cord. Glia **25,** 56, 1999.
41. Syková, E., Roitbak, T., Mazel, T., Simonová, Z. and Harvey, A.R. Astrocytes, oligodendroglia, extracellular space volume and geometry in rat fetal brain grafts. Neuroscience (in press).
42. Roitbak, T., Simonová, Z. and Syková, E. Increase in extracellular space volume and tortuosity during astrogliosis in rat cortex. European Meeting on Glial Cell Function in Health and Disease, Athens, p. 146, 1998.
43. Giftochristos, N., and David, S. Laminin and heparan sulphate proteoglycan in the lesioned adult mammalian central nervous system and their possible relationship to axonal sprouting. J. Neurocytol. **17,** 385, 1988.
44. Collins, G.H., and West N.R. Glial activity during axonal regrowth following cryogenic injury of rat spinal cord. Brain Res. Bull. **22,** 71, 1989.
45. Frisen, J., Haegerstrand, A., Risling, M., Fried, K., Johansson, C.B., Hammarberg, H., Elde, R., Hokfelt, T., and Cullheim, S. Spinal axons in the central nervous system scar tissue are closely related to laminin-immunoreactive astrocytes. Neuroscience **65,** 293, 1995.
46. Hatten, M.E., Liem, R.K., Shelanski, M.L., and Mason C.A. Astroglia in CNS injury. Glia **4,** 233, 1991.
47. Ard, M.D., Schachner M., Rapp, J.T., and Faissner, A. Growth and degeneration of axons on astrocyte surfaces: Effects on extracellular matrix and on later axonal growth. Glia **9,** 248, 1993.

48. Muller, H.W., Junghans, U., and Kappler, J. Astroglial neurotrophic and neurite-promoting factors. Pharmacol. Ther. **65,** 1, 1995.
49. Ridet, J.L., Malhotra, S.K., Privat, A., and Gage, F.H. Reactive astrocytes: Cellular and molecular cues to biological function. Trends Neurosci. **20,** 570, 1997.
50. Benowitz, L.I., and Routtenberg, A. GAP-43: An intrinsic determinant of neuronal development and plasticity. Trends Neurosci. **20,** 84, 1997.
51. Salgado-Ceballos, H., Guizar-Sahagun, G., Feria-Velasco, A., Grijalva, I., Espitia, L., and Madrazo, I. Spontaneous long-term remyelination after traumatic spinal cord injury in rats. Brain Res **782,** 126, 1998.
52. Zhang, Z., Krebs, C.J., and Guth, L. Experimental analysis of progressive necrosis after spinal cord trauma in the rat: Etiological role of inflammatory response. Exp. Neurol. **143,** 141, 1997.
53. Frisen, J. Determinants of axonal regeneration. Histol. Histopathol. **12,** 857, 1997.
54. Das, G. Perspectives in anatomy and pathology of paraplegia in experimental animals. Brain Res. Bull. **22,** 7, 1989.
55. Woerly, S., Doan, V.D., and Peduzzi, J. Experimental spinal cord reconstruction using a PHPMA hydrogel (Neurogel™) after a chronic compression injury (in preparation).
56. Woerly, S., Maghami, G., Duncan, R., Subr, V., and Ulbrich, K. Synthetic polymer derivatives as substrata for neuronal adhesion and growth. Brain Res. Bull. **30,** 423, 1993.
57. Woerly, S., Laroche, G., Marchand, R., Pato, J., Subr, V., and Ulbrich, K. Intracerebral implantation of hydrogel-coupled adhesion peptide: tissue reaction. J Neural Transpl. Plast. **5,** 245, 1995.
58. Woerly, S., Plant, G., and Harvey, A.R. Cultured rat neuronal and glial cells entrapped within hydrogel polymer matrices: A potential tool for neural tissue replacement. Neurosci. Lett. **205,** 197, 1996.
59. Harvey, A.R. Use of cell/polymer hybrid structures as conduits for regenerative growth in the CNS. In: Saunders, N.R., ed. Degeneration and Regeneration in the Nervous System. Harwood Academic Press 1999 (in press).

Address reprint requests to:
Dr. Stéphane Woerly
Organogel Canada Ltée
1400 Blvd du Parc Technologique
Quebec City, Quebec
G1P 4R7 Canada

E-mail: http://www.organogelicom.